Three-dimensional Energetic Dynamic Model of the Tire-Soil Interaction

Roberto Zanasi[1], Federica Grossi[1] and Riccardo Morselli[2]

[1]DII, University of Modena and Reggio Emilia
Via Vignolese 905, 41100 Modena, Italy, (roberto.zanasi@unimore.it)
[2]Innovation Competence Center CNH Italia S.p.A.
V.le delle Nazioni, 55 41100 Modena, Italy (riccardo.morselli@cnh.com)

***Abstract*— In the paper a three-dimensional dynamic model of the tire-soil interaction is presented. The Power-Oriented Graphs (POG) technique is used for modelling the system. An important feature of the proposed model is the use of an elastic element for describing the interaction of the tire with the ground. The proposed model solve some particular limits of the Pacejka formulas. For example it can be used also when the car or wheel velocities are zero or when the vehicle is at rest on an inclined surface. Moreover, the skidding and the slipping phenomena that in the Pecejka's formulas are mixed, in the proposed model are kept separate so allowing a more direct correspondence of the model with the physical meaning of the described phenomena. The effectiveness of the proposed model has been tested in simulation on a four wheel car.**

I. Introduction

Friction force at the tire-soil interface is the main mechanism to convert motor torque to longitudinal force. The traditional approach to this interaction involves Pacejka's formulas [1]. These formulas are based on empirical data fitting and have some limits to their applicability. In fact they are static functions which involve a great number of parameters that have to be set in function of different conditions such as road surface, tire pressure, vehicle load etc. Moreover they always require the presence of a slip to generate forces, but in this way it is not possible, for example, to simulate a vehicle at rest on an inclined surface. In this paper the Power-Oriented Graphs technique is used for modelling the elastic interaction of the tire with the soil. The three-dimensional dynamic model obtained using this energetic approach seems to be a good substitute of the Pacejka's formulas without the drawbacks previously mentioned. The paper is organized in the following way. Section II states the basic properties of the POG modelling technique. Section III shows the main features and drawbacks of the Pacejka's formulas. The POG dynamic model of the tire-soil interaction is presented in Section IV and some simulation results are given in Section V. Finally, some conclusions are reported in Section VI.

II. The bases of Power-Oriented Graphs

The "Power-Oriented Graphs" are "signal flow graphs" combined with a particular "modular" structure essentially based on the two blocks shown in Fig. 1. The basic characteristic of this modular structure is the direct correspondence between pairs of system variables and real power flows: the product of the two variables involved in each dashed line of the graph has the physical meaning of "power flowing through the section". The two basic blocks shown in Fig. 1

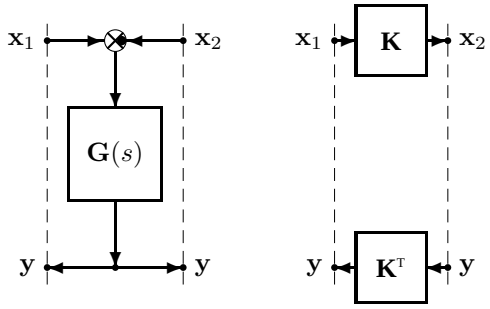

Fig. 1. Basic blocks: elaboration block (e.b.) and connection block (c.b.).

are named "elaboration block" (e.b.) and "connection block" (c.b.). The circle present in the e.b. is a summation element and the black spot represents a minus sign that multiplies the entering variable. There is no restriction on $\mathbf{x}$ and $\mathbf{y}$ other than the fact that the inner product $\langle \mathbf{x}, \mathbf{y} \rangle = \mathbf{x}^{\mathrm{T}}\mathbf{y}$ must have the physical meaning of a "power".

The e.b. and the c.b. are suitable for representing both scalar and vectorial systems. In the vectorial case, $\mathbf{G}(s)$ and $\mathbf{K}$ are matrices: $\mathbf{G}(s)$ is always square, $\mathbf{K}$ can also be rectangular. While the elaboration block can store and dissipate energy (i.e. springs, masses and dampers), the connection block can only "transform" the energy, that is, transform the system variables from one type of energy-field to another (i.e. any type of gear reduction). Please refer to [3], [4] and [5] for further details. A list of references of examples of application of the POG technique can be found in [6].

III. The tire-soil interaction: the Pacejka approach

Let's consider the bicycle model shown in Fig.2. The

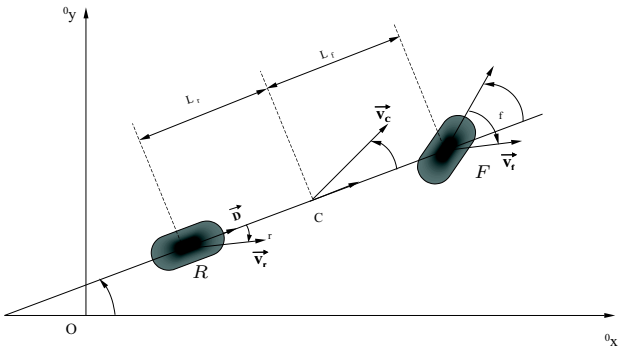

Fig. 2. Bicycle model of a rear traction vehicle.

slip-ratio $\lambda = \lambda_a$ of each wheel is defined as follows:

$$\lambda = \lambda_a = \frac{\omega R - v_x}{v_x} \tag{1}$$

where v_x and v_y represent the velocities of the wheel at the soil contact point in the direction of the tire axes x and y, ω is the angular velocity of the wheel and R is the rolling radius of the tire. In the literature one can also find the *slip-ratio* λ defined as

$$\lambda = \lambda_b = \frac{\omega R - v_x}{\omega R} \tag{2}$$

Both the definitions (1) and (2) can be used only when the denominators are positive: $v_x > 0$ and $\omega R > 0$. This limitation can be overcome taking the absolute value of the denominators:

$$\lambda_a = \frac{\omega R - v_x}{|v_x|}, \qquad \lambda_b = \frac{\omega R - v_x}{|\omega R|} \tag{3}$$

Note that the *slip-ratio* λ_a cannot be used when $v_x = 0$ (the tire rotates without translating) and λ_b cannot be used when $\omega = 0$ (the tire translates without rotating).

Pacejka's *magic formulas* [1] are usually used to calculate the longitudinal force F_x, the lateral force F_y and the self-aligning torque M_z of each tire as a function of the *slip-ratio* λ, the *slip-angle* $\alpha = \arctan \frac{v_y}{v_x}$, the *vertical load* F_z and the *camber angle* γ (see Fig. 3 for forces F_x and F_y). A limit of these formulas is the fact that they provide zero forces and torques when the slip-ratio λ is zero and in some cases they do not work correctly such as for example when the vehicle is stopped on an inclined surface: in fact in this case the slip-ratio is zero, but a longitudinal force must be present to keep the vehicle at rest on the inclined surface. Moreover Pacejka's formulas mix together the "slip" and "skid" phenomena, in fact for small values of λ these formulas essentially describe the "slip" of the tire due to the rolling of the wheel when a force is generated at the ground, while for large values of λ the same formulas mainly describe the "skidding" of the wheel when the tire loses the adherence to the ground.

A weak point of definitions (3) is the fact that they are not symmetric with respect to the terms v_x and ωR, that is they

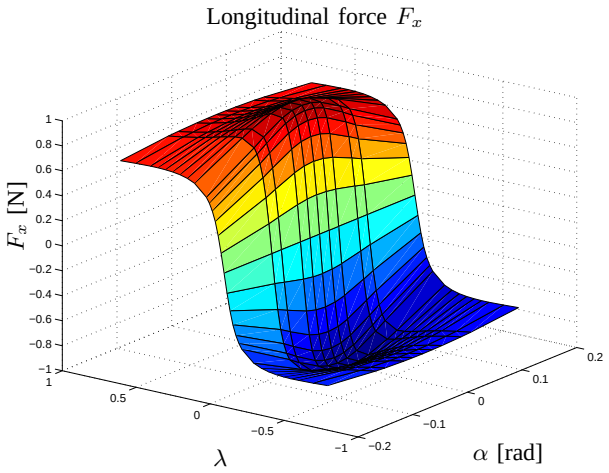

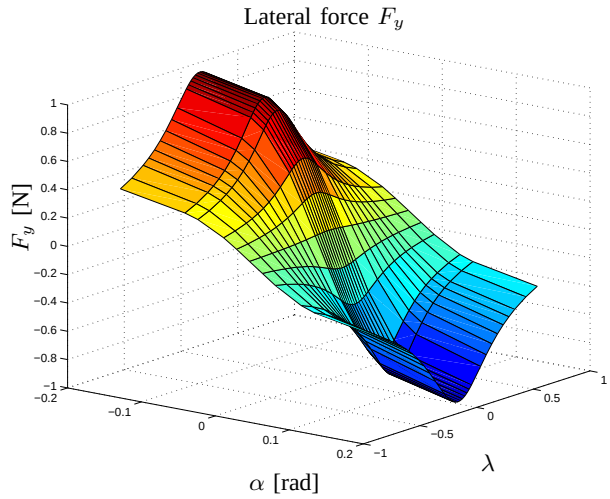

Fig. 3. Modulus of forces F_x and F_y normalized with respect to a constant vertical load N_z.

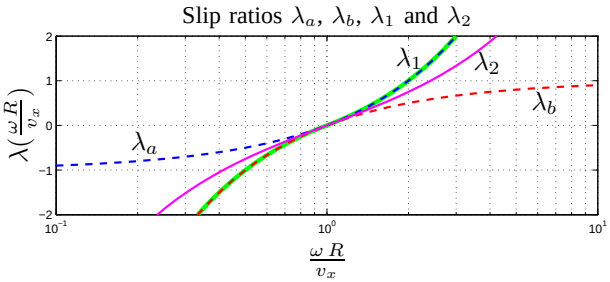

Fig. 4. Four different definitions of the slip ratio λ as a function of $\frac{\omega R}{v_x}$: λ_a, λ_b, λ_1 and λ_2.

have quite different behaviours when $v_x \to 0$ and $\omega \to 0$. Alternative definitions for the *slip-ratio* which behave in a symmetric way with respect to v_x and ω are the following:

$$\lambda_1 = \frac{\omega R - v_x}{\min(|\omega R|, |v_x|)}, \tag{4}$$

and

$$\lambda_2 = \frac{\omega R - v_x}{2}\left(\frac{1}{|\omega R|} + \frac{1}{|v_x|}\right) \tag{5}$$

A comparison between the four different definitions λ_a, λ_b, λ_1 and λ_2 as function of the ratio $\frac{\omega R}{v_x}$ is shown in Fig. 4 where the picture has been drawn in semi-logarithmic scale. Note that all these definitions of slip ratio act in the same way in the vicinity of the point $\frac{\omega R}{v_x}$. When $\frac{\omega R}{v_x} \to 0$ variables λ_1, λ_2 and λ_b tend to $-\infty$ and λ_a goes to -1, when $\frac{\omega R}{v_x} \to \infty$ variables λ_1, λ_2 and λ_a tend to $+\infty$ and λ_b goes to 1.

The typical graphical shape of the Pacejka's formula when $\alpha = 0$ is shown in Fig. 5. This formula gives the

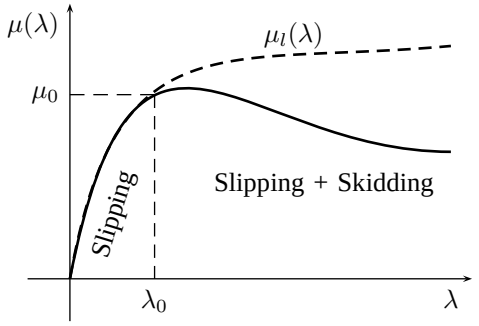

Fig. 5. The typical shape of the Pacejka's formula when $\alpha = 0$.

friction coefficient $\mu = \frac{f_x}{f_z}$ (f_x and f_z are the longitudinal and normal contact forces) as a function of the slip ratio λ. Note that when $\lambda < \lambda_0$ the tire-soil interaction is only "slipping", while when $\lambda > \lambda_0$ the interaction is also "skidding".

IV. The tire-soil interaction: the energetic approach

Notations: symbols $[\vec{\mathbf{a}}\times]$, $[\![\vec{\mathbf{a}}]\!]$ and $\mathbf{A}\bullet$ are defined as follows:

$$\vec{\mathbf{a}} = \begin{bmatrix} a_x \\ a_y \\ a_z \end{bmatrix}, \qquad [\vec{\mathbf{a}}\times] = \begin{bmatrix} 0 & -a_z & a_y \\ a_z & 0 & -a_x \\ -a_y & a_x & 0 \end{bmatrix}$$

$$[\![\vec{\mathbf{a}}]\!] = \begin{bmatrix} \mathbf{I}_3 & \mathbf{0} \\ [\vec{\mathbf{a}}\times] & \mathbf{I}_3 \end{bmatrix}, \qquad \mathbf{A}\bullet = \begin{bmatrix} \mathbf{A} & \mathbf{0} \\ \mathbf{0} & \mathbf{A} \end{bmatrix}$$

where $\mathbf{I}_3$ and $\mathbf{0}$ are the 3×3 identity and zero matrices. The modulus of vector $\mathbf{x}$ will be denoted as $|\mathbf{x}|$.

The POG energetic approach. Let us consider the dynamic system shown in Fig. 6 composed by a wheel with an elastic interaction with the ground. The dynamic model of this system described by using the Power-Oriented Graphs technique is shown in Fig.8. This POG scheme puts in evidence how the powers flow through the system by using a six-dimensional vectorial notation. The power section ① of the POG scheme is characterized by the force and velocity vectors ${}^0\vec{\mathbf{F}}_{r0}$ and ${}^0\vec{\mathbf{V}}_{r0}$ of point r_0 (i.e. the center of mass of the wheel) expressed in the inertial frame Σ_0.

Coordinate transformation: $\Sigma_0 \to \Sigma_r$. The unitary matrix ${}^r\mathbf{R}_0 \in \mathbf{R}^{3\times3}$ present in the connection block between power sections ① and ② is the rotation matrix which transforms vectors from the inertial frame Σ_0 to the frame

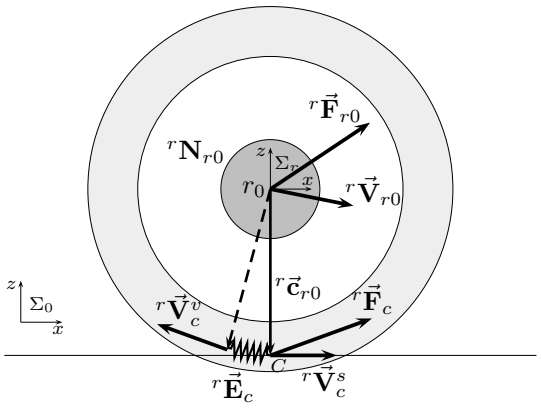

Fig. 6. The considered system: a wheel with an elastic interaction with the ground.

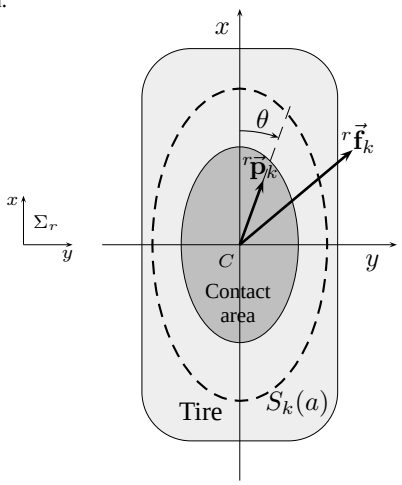

Fig. 7. The contact area of the tire on the ground.

Σ_r rigidly connected to the wheel and with its origin in r_0. Vectors ${}^r\vec{\mathbf{F}}_{r0}$ and ${}^r\vec{\mathbf{V}}_{r0}$ which characterize the power section ② denote the force and velocity vectors of point r_0 expressed in frame Σ_r. They are defined as follows:

$${}^r\vec{\mathbf{F}}_{r0} = \begin{bmatrix} {}^r\vec{\mathbf{f}}_{r0} \\ {}^r\vec{\tau}_{r0} \end{bmatrix}, \qquad {}^r\vec{\mathbf{V}}_{r0} = \begin{bmatrix} {}^r\vec{\mathbf{v}}_{r0} \\ {}^r\vec{\omega}_{r0} \end{bmatrix}$$

where ${}^r\vec{\mathbf{f}}_{r0}$, ${}^r\vec{\tau}_{r0}$, ${}^r\vec{\mathbf{v}}_{r0} = [{}^r v_{r0x},\ {}^r v_{r0y},\ {}^r v_{r0z}]^{\mathrm{T}}$ and ${}^r\vec{\omega}_{r0} = [{}^r\omega_{r0x},\ {}^r\omega_{r0y},\ {}^r\omega_{r0z}]^{\mathrm{T}}$ are the force, the torque, the linear and angular velocity vectors of point r_0.

The mechanical dynamics. The POG elaboration blocks present between power sections ② and ③ represent the mechanical dynamics of the wheel. Matrix ${}^r\mathbf{N}_{r0}$ is the six-dimensional mass-inertia matrix of the wheel expressed in frame Σ_r:

$${}^r\mathbf{N}_{r0} = \begin{bmatrix} \mathbf{M}_r & \mathbf{0} \\ \mathbf{0} & {}^r\mathbf{J}_r \end{bmatrix}$$

and

$$\mathbf{M}_r = \begin{bmatrix} m_r & & \\ & m_r & \\ & & m_r \end{bmatrix}, \ {}^r\mathbf{J}_r = \begin{bmatrix} J_{rx} & & \\ & J_{ry} & \\ & & J_{rz} \end{bmatrix}$$

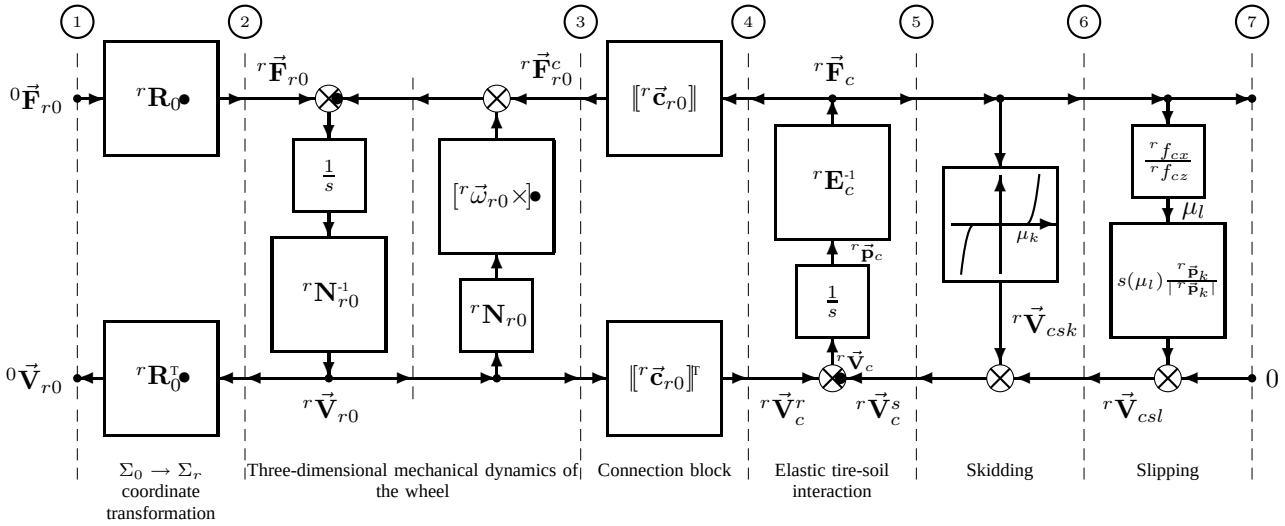

Fig. 8. The POG dynamic model of the wheel and the elastic tire-soil interaction.

where m_r is the mass of the wheel and J_{rx}, J_{ry}, J_{rz} are the principal axes inertia momenta of the wheel. The dynamics of the wheel in the "inertial" frame Σ_0 is described by the "Newton's" equation $^0\vec{\mathbf{F}}^t_{r0} = \frac{d}{dt}(\,^0\mathbf{N}_{r0}\,^0\vec{\mathbf{V}}_{r0})$ where $^0\vec{\mathbf{F}}^t_{r0}$ is the total force acting on the center of mass of the wheel. It can be shown that this equation can be transformed into

$$^r\vec{\mathbf{F}}^t_{r0} = [^r\vec{\omega}_{r0}\times]\bullet\,^r\mathbf{N}_{r0}\,^r\vec{\mathbf{V}}_{r0} + \tfrac{d}{dt}(\,^r\mathbf{N}_{r0}\,^r\vec{\mathbf{V}}_{r0})$$

where, for the considered system, the total force $^r\vec{\mathbf{F}}^t_{r0} = {}^r\vec{\mathbf{F}}_{r0} - {}^r\vec{\mathbf{F}}^c_{r0}$ is the sum of the external forces $^r\vec{\mathbf{F}}_{r0}$ and the contact forces $^r\vec{\mathbf{F}}^c_{r0}$ expressed in the reference frame Σ_r.

Connection block: $r_0 \rightarrow c$. For a rigid body, a force $^r\vec{\mathbf{F}}_c$ applied to point c can be transformed to the equivalent force $^r\vec{\mathbf{F}}_{r0}$ applied to point r_0 by using the following transformation matrix $[\![^r\vec{\mathbf{c}}_{r0}]\!]$:

$$^r\vec{\mathbf{F}}_{r0} = [\![^r\vec{\mathbf{c}}_{r0}]\!]\,^r\vec{\mathbf{F}}_c = \begin{bmatrix} \mathbf{I}_3 & \mathbf{0} \\ [^r\vec{\mathbf{c}}_{r0}\times] & \mathbf{I}_3 \end{bmatrix} \begin{bmatrix} ^r\vec{\mathbf{f}}_c \\ ^r\vec{\tau}_c \end{bmatrix}. \quad (6)$$

For duality the transpose matrix $[\![^r\vec{\mathbf{c}}_{r0}]\!]^{\mathrm{T}}$ relates velocity $^r\vec{\mathbf{V}}_{r0}$ to velocity $^r\vec{\mathbf{V}}^r_c$:

$$^r\vec{\mathbf{V}}^r_c = [\![^r\vec{\mathbf{c}}_{r0}]\!]^{\mathrm{T}}\,^r\vec{\mathbf{V}}_{r0} = \begin{bmatrix} \mathbf{I}_3 & [^r\vec{\mathbf{c}}_{r0}\times]^{\mathrm{T}} \\ \mathbf{0} & \mathbf{I}_3 \end{bmatrix} \begin{bmatrix} ^r\vec{\mathbf{v}}_{r0} \\ ^r\vec{\omega}_{r0} \end{bmatrix}. \quad (7)$$

Both the transformations (6) and (7) are present in POG scheme of Fig.8 in the connection block between the power sections ③ and ④.

The elastic dynamics. The dynamics of the elastic interaction of the tire with the ground is represented by the POG elaboration block present between sections ④ and ⑤. This elastic dynamics is described by the equation $^r\vec{\mathbf{V}}_c = \frac{d}{dt}(\,^r\mathbf{E}_c\,^r\vec{\mathbf{F}}_c)$ where $^r\vec{\mathbf{V}}_c = {}^r\vec{\mathbf{V}}^r_c - {}^r\vec{\mathbf{V}}^s_c$ is the difference between the rolling $^r\vec{\mathbf{V}}^r_c$ and sliding $^r\vec{\mathbf{V}}^s_c$ velocities of the contact point c. Matrix $^r\mathbf{E}_c$ ($^r\mathbf{K}_c^{-1}$) is the six-dimensional elasticity (stiffness) matrix of the tire-soil contact area (see Fig. 7 centered in point c:

$$^r\mathbf{E}_c = \begin{bmatrix} ^r\mathbf{E}^t_c & \mathbf{0} \\ \mathbf{0} & ^r\mathbf{E}^r_c \end{bmatrix} = {}^r\mathbf{K}_c^{-1} \quad (8)$$

and

$$(\,^r\mathbf{E}^t_c)^{-1} = \begin{bmatrix} k_x & & \\ & k_y & \\ & & k_z \end{bmatrix}, \qquad (^r\mathbf{E}^r_c)^{-1} = \begin{bmatrix} 0 & & \\ & 0 & \\ & & k_{mz} \end{bmatrix} \quad (9)$$

where k_x, k_y, k_z, k_{mz} are the translational and rotational stiffness coefficients of the tire-soil contact area. Note that in (8) the structure of matrices $^r\mathbf{E}^t_c$ and $^r\mathbf{E}^r_c$ is a particular case used for this study, but in the general case they are full matrices. Matrix $^r\mathbf{E}_c^{-1}$ relates the elastic displacement $^r\vec{\mathbf{p}}_c = [\,^rp_{cx},\ ^rp_{cy},\ ^rp_{cz},\ ^r\delta_{cx},\ ^r\delta_{cy},\ ^r\delta_{cz}]^{\mathrm{T}}$ to the force $^r\vec{\mathbf{F}}_c$ generated in the contact point c:

$$^r\vec{\mathbf{F}}_c = \begin{bmatrix} ^rf_{cx} \\ ^rf_{cy} \\ ^rf_{cz} \\ 0 \\ 0 \\ ^r\tau_{cz} \end{bmatrix} = {}^r\mathbf{E}_c^{-1}\,^r\vec{\mathbf{p}}_c = \begin{bmatrix} k_x\,^rp_{cx} \\ k_y\,^rp_{cy} \\ k_y\,^rp_{cz} \\ 0 \\ 0 \\ k_{mz}\,^r\delta_{cz} \end{bmatrix}.$$

The six-dimensional elastic element $^r\mathbf{E}_c^{-1}$ located in the contact point c is characterized at an end by the rolling velocity $^r\vec{\mathbf{V}}^r_c$ of the tire and at the other end by the sliding velocity $^r\vec{\mathbf{V}}^s_c$ due to the "skidding" and "slipping" phenomena: $^r\vec{\mathbf{V}}^s_c = {}^r\vec{\mathbf{V}}_{csk} + {}^r\vec{\mathbf{V}}_{csl}$ (see Fig. 8).

The skidding. The POG elaboration block present between power sections ⑤ and ⑥ describes the "skidding" of the tire on the ground. Let $^r\vec{\mathbf{p}}_k = [\,^rp_{cx},\ ^rp_{cy},\ 0,\ 0,\ 0,\ ^r\delta_{cz}]^{\mathrm{T}}$ and $^r\vec{\mathbf{f}}_k = [\,^rf_{cx},\ ^rf_{cy},\ 0,\ 0,\ 0,\ ^r\tau_{cz}]^{\mathrm{T}}$ denote the orthogonal projection of the displacement and force vectors $^r\vec{\mathbf{p}}_c$ and $^r\vec{\mathbf{F}}_c$ on the three-dimensional subspace composed by the contact plane x-y where the tire interacts with the ground

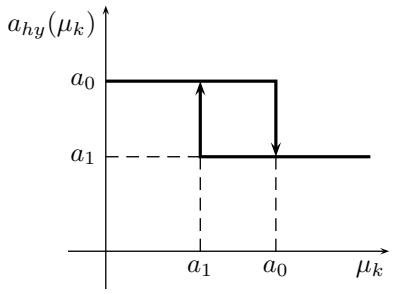

Fig. 9. Hysteresis function: the input a_{hy} of the linear filter (13) is a function of the parameter $\mu_k({}^r\vec{\mathbf{F}}_c)$ defined in (11).

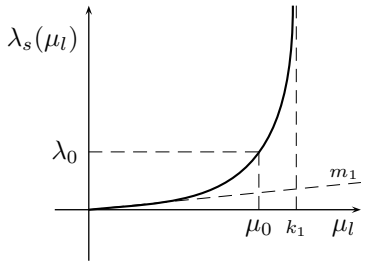

Fig. 10. Slipping function $\lambda_s(\mu_l)$ that describes the slip ratio λ_s as a function of the friction coefficient μ_l.

and the direction z of the torsional displacement and momentum. In the general case vectors ${}^r\vec{\mathbf{p}}_k$ and ${}^r\vec{\mathbf{f}}_k$ are not parallel, see Fig. 7. The tire starts skidding when the vector ${}^r\vec{\mathbf{f}}_k$ exceeds a *skidding ellipsoid* S_k defined as follows:

$$S_k({}^r\vec{\mathbf{F}}_c,\, a) = \left\{ {}^r\vec{\mathbf{f}}_k \;:\; \mu_k({}^r\vec{\mathbf{F}}_c) = a \right\} \tag{10}$$

where

$$\mu_k({}^r\vec{\mathbf{F}}_c) = \sqrt{\left(\frac{{}^r f_{cx}}{{}^r f_{cz}}\right)^2 + \left(\frac{{}^r f_{cy}}{\gamma_y\, {}^r f_{cz}}\right)^2 + \left(\frac{{}^r \tau_{cz}}{\gamma_m\, {}^r f_{cz}}\right)^2}. \tag{11}$$

The parameters a, $\gamma_y a$ and $\gamma_m a$ are the half lengths of the principal axes of the *skidding ellipsoid* $S_k({}^r\vec{\mathbf{F}}_c,\, a)$: parameter a is used to linearely expand or contract the dimension of the ellipsoid, while parameters γ_y and γ_m can be used to properly define its shape. The dashed line shown in Fig. 7 represents the intersection of the *skidding ellipsoid* S_k with the x-y contact plane. Function $\mu_k({}^r\vec{\mathbf{F}}_c)$ is a normalized measure of the distance of vector ${}^r\vec{\mathbf{f}}_k$ from the *skidding ellipsoid* S_k: when $\mu_k < a$ the vector is inside the ellipsoid, when $\mu_k > a$ the vector is outside. The skidding velocity ${}^r\vec{\mathbf{V}}_{csk} = [{}^rV_{kx},\, {}^rV_{ky},\, 0,\, 0,\, 0,\, {}^r\omega_{kz}]$ of the contact point c can be defined as follows:

$${}^r\vec{\mathbf{V}}_{csk} = \begin{cases} 0 & \text{if } \mu_k({}^r\vec{\mathbf{F}}_c) \le a \\ K_s\Big(\mu_k({}^r\vec{\mathbf{F}}_c) - a\Big)^2 \dfrac{{}^r\vec{\mathbf{p}}_k}{|{}^r\vec{\mathbf{p}}_k|} & \text{otherwise} \end{cases} \tag{12}$$

where K_s is a proper positive coefficient and a is the output of a first order linear filter:

$$\dot{a} = \frac{1}{\tau_{hy}}(a_{hy} - a) \tag{13}$$

characterized by the time constant τ_{hy} and by the input $a_{hy} = a_{hy}(\mu_k)$ shown in Fig. 9. From (12) it is evident that the skidding velocity ${}^r\vec{\mathbf{V}}_{csk}$ always has the same direction of the displacement vector ${}^r\vec{\mathbf{p}}_k$: this means that the skidding is always described as a dissipative phenomenon. The quadratic function $K_s\Big(\mu_k({}^r\vec{\mathbf{F}}_c) - a\Big)^2$ used in (12) is "one" of the possible functions that can be used outside the ellipsoid to force the vector ${}^r\vec{\mathbf{f}}_k$ to quickly enter back into the skidding ellipsoid: other positive monotonic increasing functions could also be used.

The slipping. The POG elaboration block present between power sections ⑥ and ⑦ describes the "slipping" of the tire on the ground. The tire slips on the ground only when both the contact force ${}^r f_{cx}$ in the x-direction and the angular velocity of the wheel ${}^r\omega_{r0y}$ in the y-direction are not zero. The slipping velocity ${}^r\vec{\mathbf{V}}_{csl} = [{}^rV_{lx},\, {}^rV_{ly},\, 0,\, 0,\, 0,\, {}^r\omega_{lz}]$ of the contact point c can be defined as follows:

$${}^r\vec{\mathbf{V}}_{csl} = \min(|\,{}^r\omega_{r0y}\, R_e|, |\,{}^rv_{r0x}|)\; |\lambda_s(\mu_l)|\; \frac{{}^r\vec{\mathbf{p}}_k}{|\,{}^r\vec{\mathbf{p}}_k|} \tag{14}$$

where $R_e = |\,{}^r\vec{\mathbf{c}}_{r0}|$ is the effective rolling radius of the wheel, $\mu_l = \frac{{}^r f_{cx}}{{}^r f_{cz}}$ is the modulus of the friction coefficient of the contact point c in the x direction and function $\lambda_s(\mu_l)$ if the inverse of the function $\mu_l(\lambda)$ that in the Pacejka's formula expresses the μ coefficient as a function of the slip ratio λ, see Fig. 5. The function $\lambda_s(\mu_l)$ that describes the slipping behaviour has a shape (which depends on complex physical phenomena) that can be fitted, for example, by the following function:

$$\lambda_s(\mu_l) = \frac{m_1\, \mu_l}{1 - \left(\frac{\mu_l}{k_1}\right)^2} \tag{15}$$

where coefficients m_1 and k_1 describes respectively the slope in the origin and the ascissa of the asymptote of the function, see Fig. 10. From (14) it is evident that also the slipping phenomenon is described as "dissipative", in fact also the slipping velocity ${}^r\vec{\mathbf{V}}_{csl}$ always has the same direction of the displacement vector ${}^r\vec{\mathbf{p}}_k$. The structure of eq. (14) has been obtained from the definition (4) of the slip ratio λ_1 substituting λ_1 with $\lambda_s(\mu_l)$ and the term $(\omega\, R - v_x)$ with the velocity ${}^r\vec{\mathbf{V}}_{csl}$. In this way one obtains that the slipping velocity ${}^r\vec{\mathbf{V}}_{csl}$ is zero when ${}^r\omega_{r0y} = 0$ and when ${}^rv_{r0x} = 0$, as desired. A similar definition for the slipping velocity ${}^r\vec{\mathbf{V}}_{csl}$ could also be obtained referring to definition (5) of the slip ratio λ_2.

V. Simulations

The dynamic behaviour of the proposed model for the tire-soil interaction has been tested in simulation on a four wheel car: a view of the considered car in Virtual Reality environment is shown in Fig. 11. The Simulink-SimMechanics block scheme of the considered four wheel

car is shown in Fig. 12. The grey blocks represent the mechanical dynamics of the wheels, while the green blocks implement the dynamics of the tire-soil interaction as it has been described in Sec. IV.

Fig. 11. A view of the modelled four wheel car in Virtual Reality environment.

The main parameters used in simulation are the following: $m_c = 1192$ kg mass of the vehicle body; $m_r = 40$ kg mass of each wheel; $[J_{rx}, J_{ry}, J_{rz}] = [0.885, 1.279, 0.885]$ kg m^2 inertia momenta of each wheel; $R = 0.325$ m radius of each wheel; $L_s = 2.52$ m distance between front and rear axle shafts; $L_w = 1.5$ m distance between left and right wheels; $K_{sp} = 80000$ N/m, $b_{sp} = 3000$ N s/m stiffness and friction coefficients of the suspensions; $b_{rol} = 40$ N m s/rad rolling friction coefficient of the wheels; $[k_x, k_y, k_z] = [360000, 360000, 250000]$ N/m, $k_{mz} = 1800$ N m/rad translational and rotational stiffness coefficients of the tire; $\gamma_y = 0.7$, $\gamma_m = 2$, $K_s = 60$ parameters of the skidding velocity ${}^r\vec{\mathbf{V}}_{csk}$ defined in (12); $\tau_{hy} = 0.02$ s time constant of the linear filter (13); $a_0 = 0.9$, $a_1 = 0.5$ parameters of function $a_{hy}(\mu_k)$ defined in Fig. 9; $m_1 = 0.04$, $k_1 = 1.21$ parameters of the slipping function $\lambda_s(\mu_l)$ defined in (15). At $t = 0$ the suspensions and the tires are unloaded. The car is excited with a steering torque $T_{st}(t)$:

$$T_{st}(t) = 400\ \cos(t)\ \text{Nm}$$

and with a traction torque $T_{tr}(t)$:

$$T_{tr}(t) = 1000(1 - \cos(2t))\ \text{Nm}$$

applied on both the front wheels. The torque $T_{st}(t)$ is used to steer the front wheels. The steering angle $\delta(t)$ of the car is shown in the upper part of Fig. 13. The amplitude of the sinusoidal traction torque $T_{tr}(t)$ is high enough to accelerate the car from zero to 15 km/h, see the lower part of Fig. 13, and to cause the skidding of the front wheels. All the simulation results reported in the following figures (from Fig. 14 to Fig. 21) refer only to the front left wheel of the car. The forces ${}^r f_{cx}$, ${}^r f_{cy}$, ${}^r f_{cz}$ that the tire applies to the ground at the contact point C are shown in Fig. 14. The oscillation of the normal force ${}^r f_{cz}$ in the first part of the simulation is due to the initial settling dynamics of the suspensions. The forces ${}^r f_{cx}$ and ${}^r f_{cy}$ acting on the ground in x and y directions are the sum of the forces caused by both the skidding and slipping phenomena. The corresponding trajectory of the normalized force vector ${}^r\mathbf{f}_n = ({}^r f_{cx}, {}^r f_{cy})/|{}^r f_{cz}|$ moving within the skidding ellipsoid $S_k(a)$ is reported in Fig. 15: the two dashed lines show the positions of the skidding ellipsoid $S_k(a)$ when $a = a_0$ and $a = a_1$. Note that the wheel starts skidding only when the normalized vector ${}^r\mathbf{f}_n$ exceeds the ellipsoid $S_k(a_0)$ (at instants $t_1 = 0.86$ s and $t_3 = 4.1$ s) and stops skidding when the vector ${}^r\mathbf{f}_n$ enters into the ellipsoid $S_k(a_1)$ (at instant $t_2 = 2.29$ s). To help the reader, in the figures that report time behaviours of variables, the instants t_1, t_2 and t_3 are evidenced with vertical dashed magenta lines.

The skidding velocities ${}^r V_{kx}$, ${}^r V_{ky}$ and ${}^r\omega_{kz}$ generated at the contact point C are shown in Fig. 16. Note that these velocities are different from zero only when the tire is skidding. The hysteresis behaviour associated to the skidding phenomenon is clearly shown in Fig. 17: in the left part of the figure it is reported the parameter $a(\mu_k)$ which defines the amplitude of the skidding ellipsoid $S_k(a)$; the right part of the figure shows the modulus of the skidding velocity $|{}^r\vec{\mathbf{V}}_{csk}|$ as a function of parameter $a(\mu_k)$.

The slipping velocities ${}^r V_{lx}$, ${}^r V_{ly}$ and ${}^r\omega_{lz}$ at the contact point C are shown in Fig. 18. Note that the slipping velocities go to zero only when ${}^r\omega_{r0y} = 0$ or when ${}^r v_{r0x} = 0$, see definition (14). A comparison between tire velocity ${}^r\omega_{r0y} R_e$ and wheel velocity ${}^r v_{r0x}$ is proposed in Fig. 19: the two velocities are very close when the tire is only slipping while they are quite different when the tire is skidding. The time behaviour of the slip ratios $\lambda_a(t)$, $\lambda_b(t)$ and $\lambda_s(t)$ defined in (3) and in 15 are given in Fig. 20. The three slip ratios are quite different when the tire is skidding while they are quite similar when the tire is only slipping, see the zoom in the lower part of the figure. Note that during slipping the variable λ_s differs a little bit from the other two slip ratios because it is used to load and unload the elastic element which is present in the proposed dynamic model but is absent in the Pacejka static model. Fig. 21 has been obtained drawing the friction coefficient μ_l as function of the three slip ratios λ_a, λ_b and λ_s one obtains. This figure clearly shows how the proposed model is able to reproduce the typical shape of the Pacejka's formula, see Fig. 5.

VI. Conclusions

In the paper a three-dimensional dynamic model of the elastic interaction of a tire with the ground has been presented. The system has been modelled using the POG graphical technique and then implemented in Simulink-SimMechanics environment. The simulation results show that the proposed model can be a good substitute of the Pacejka's formulas avoiding some drawbacks. In particular

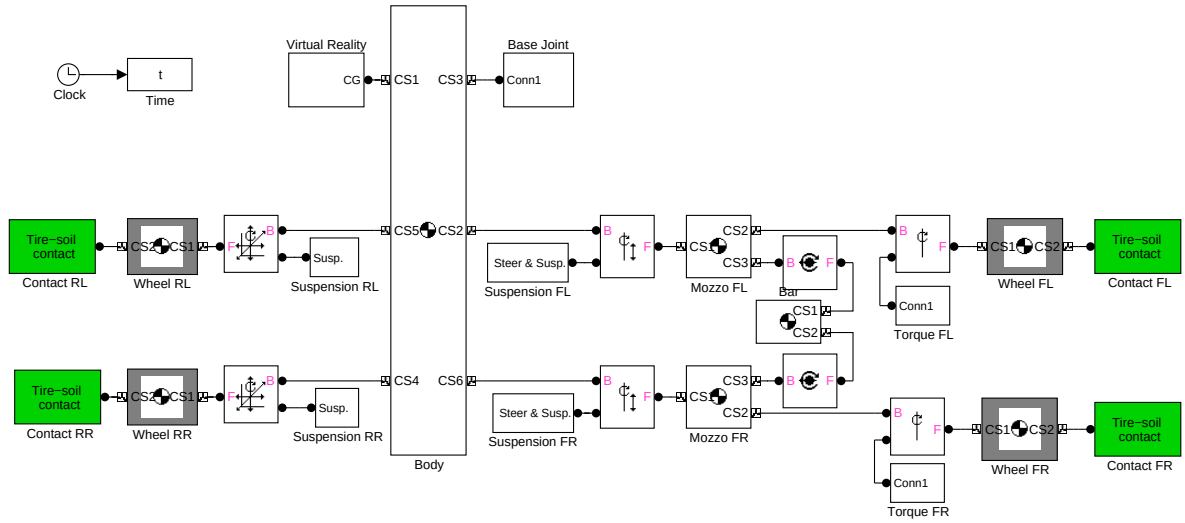

Fig. 12. The Simulink-SimMechanics block scheme of the considered four wheel car.

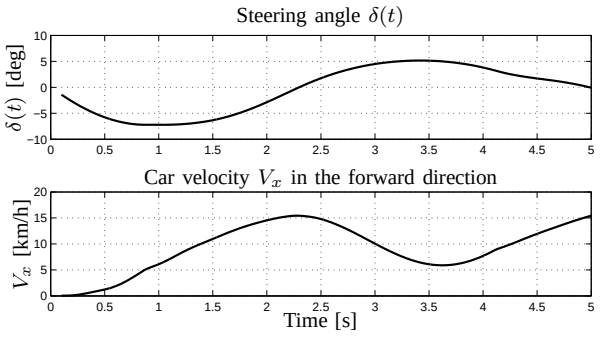

Fig. 13. Steering angle $\delta(t)$ and car velocity V_x in the forward direction.

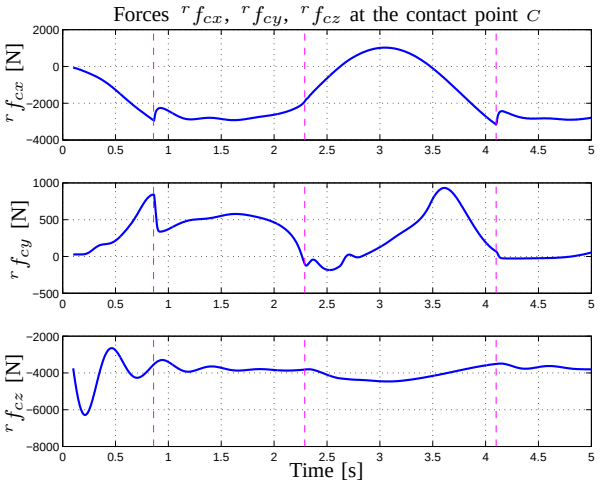

Fig. 14. Forces ${}^r f_{cx}$, ${}^r f_{cy}$, ${}^r f_{cz}$ at the contact point C.

the proposed model can also be used when the car or wheel velocities are zero or when the vehicle is at rest on an inclined surface. An important feature of the proposed model is the use of an elastic element for describing the

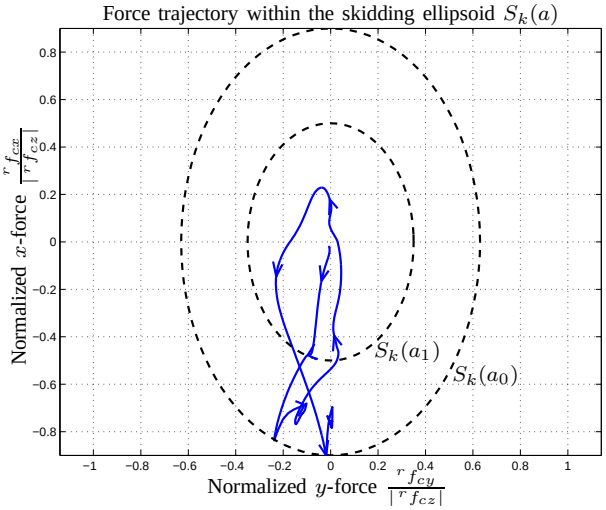

Fig. 15. Trajectory of the normalized force $({}^r f_{cx}, {}^r f_{cy})/|{}^r f_{cz}|$ within the skidding ellipsoid $S_k(a)$.

interaction of the tire with the ground. This elastic element, which surely is present in the physical system, is not considered in the Pacejka model. So, the presented model seems to be particularly suitable for the study of all the physical situations in which the presence of the tire elasticity can be important, such as, for example, the design and the tuning of the ABS and ESP control systems.

REFERENCES

[1] H.B. Pacejka, "Tire and Vehicle Dynamics", Elsevier Science, On behalf of Society of Automotive Engineers, Oxford, 2002.

[2] Paynter, H.M., *Analysis and Design of Engineering Systems*, MIT-press, Camb., MA, 1961.

[3] R. Zanasi, "Power Oriented Modelling of Dynamical System for Simulation", *IMACS Symp. on Modelling and Control of Technological System*, Lille, France, May 1991.

[4] R. Zanasi, K. Salisbury, "Dynamic Modeling, Simulation and Parameter Identifi cation for the WAM Arm", *A.I. Memo No. 1387*, MIT, Cambridge, USA, August 1992.

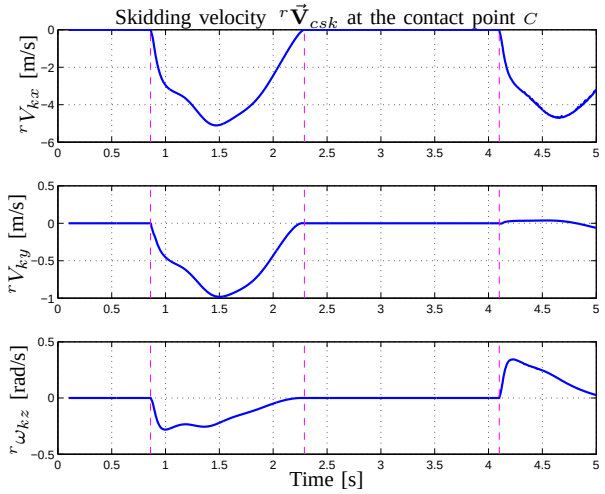

Fig. 16. Skidding velocities ${}^rV_{kx}$, ${}^rV_{ky}$ and ${}^r\omega_{kz}$ at the contact point C.

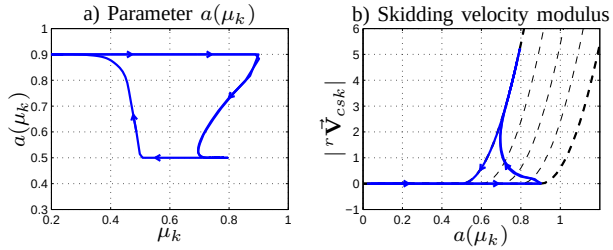

Fig. 17. Skidding phenomenon: a) parameter $a(\mu_k)$ of the skidding ellipsoid $S_k(a)$; b) modulus of the skidding velocity $|{}^r\vec{\mathbf{V}}_{csk}|$ as a function of parameter $a(\mu_k)$.

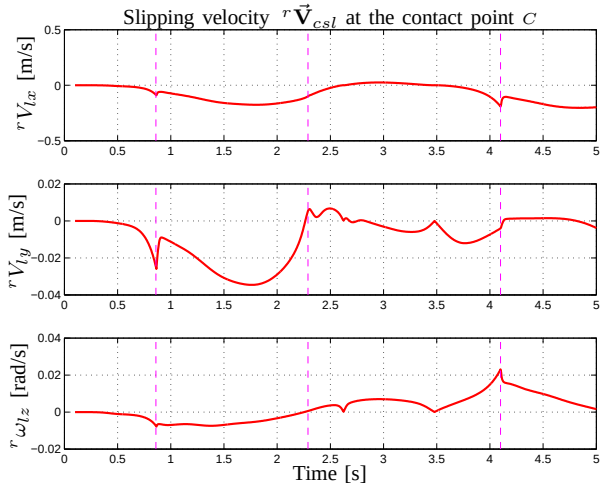

Fig. 18. Slipping velocities ${}^rV_{lx}$, ${}^rV_{ly}$ and ${}^r\omega_{lz}$ at the contact point C.

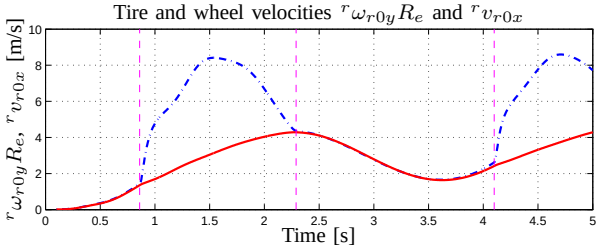

Fig. 19. Tire velocity ${}^r\omega_{r0y}R_e$ (dashdotted blue) and wheel velocity ${}^rv_{r0x}$ (solid red) at the contact point C.

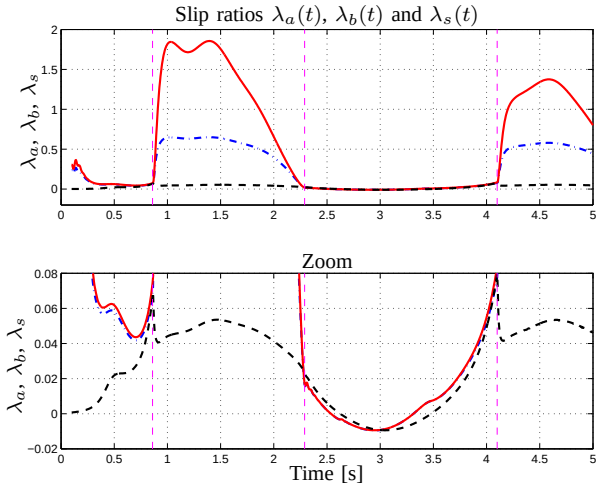

Fig. 20. Slip ratios $\lambda_a(t)$ (solid red), $\lambda_b(t)$ (dashdotted blue) and $\lambda_s(t)$ (dashed black).

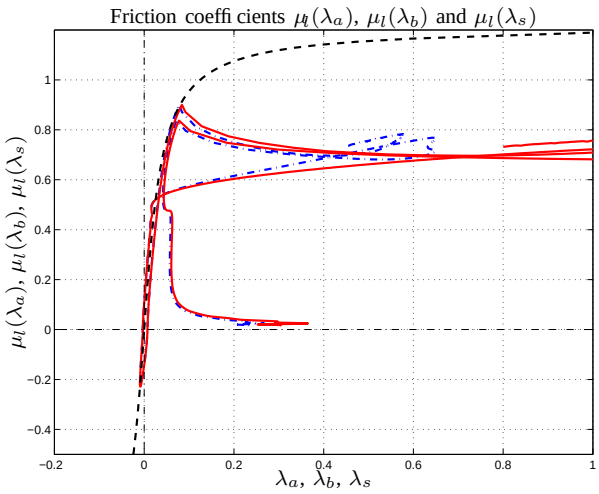

Fig. 21. Friction coeffi cients $\mu_l(\lambda_a)$ (solid red), $\mu_l(\lambda_b)$ (dashdotted blue) and $\mu_l(\lambda_s)$ (dashed black) of the contact point C.

[5] Zanasi R., "Dynamics of a n-links Manipulator by Using Power-Oriented Graph", *SYROCO '94*, Capri, Italy, 1994.

[6] R. Morselli, R. Zanasi, "Modeling of Automotive Control Systems Using Power Oriented Graphs", 32nd Annual Conference of the IEEE Industrial Electronics Society, IECON 2006, Parigi, 7-10 Nov., 2006.

[7] R. Zanasi , A. Visconti, G. Sandoni, R. Morselli, "Dynamic Modeling and Control of a Car Transmission System", *International Conference on Advanced Intelligent Mechatronics*, Como, Italy, July 8-12, 2001.

[8] R. Morselli, R. Zanasi, "A Self-Tuning ABS Control for Electro-mechanical Braking Systems", MECHATRONICS 2006, Heidelberg, 12-14 September, 2006.

[9] R. Morselli, R. Zanasi, "Control of Mechatronic Systems by Dissipative Devices: Application to Semi-Active Vehicle Suspensions", 2006 American Control Conference, ACC 2006, Minneapolis, Minnesota, USA, June 14-16, 2006.